

GENERATING QUANTUM INTERFERENCE AND POLARIZATION ENTANGLEMENT WITH OPTICAL PARAMETRIC AMPLIFIERS

JEFFREY H. SHAPIRO

*Research Laboratory of Electronics
Massachusetts Institute of Technology
Cambridge, MA 02139
E-mail: jhs@mit.edu*

A traveling-wave treatment of a type-II phase matched optical parametric amplifier (OPA) is reported. It connects the standard Gaussian-state analysis for such a system to the bi-photon wave packet characterization of a parametric downconverter. This treatment reproduces the narrowband (near-resonance) predictions of the lumped-element OPA theory for doubly-resonant operation. Without the near-resonance restriction, a new quantum interference effect emerges: coincidence-counting dips and revivals in a Hong-Ou-Mandel interferometer.

Parametric downconversion sources are intrinsically broadband; THz bandwidths are typical. Our recent proposal for long-distance qubit teleportation,¹ however, requires a high-brightness narrowband source of polarization entanglement, to match the MHz linewidth of its trapped-atom quantum memory.² We have shown theoretically³ that the polarization-combined outputs from a pair of coherently-pumped, doubly-resonant, optical parametric amplifiers (OPAs) will fulfill this need. That analysis employed a lumped-element model for the OPA behavior in the vicinity of the double resonance, and was sufficiently generic to include both type-I and type-II phase matching. In the present paper, we report a traveling-wave treatment of the type-II phase matched, doubly-resonant OPA. When restricted to frequencies close to the double resonance, the new analysis reproduces the lumped-element results. Without this restriction, however, a new quantum interference effect emerges: coincidence-counting dips and revivals in a Hong-Ou-Mandel (HOM) interferometer.⁴ Our work is related to that of Lu and Ou,⁵ who published a multi-mode lumped-element analysis for the photon statistics of type-I and type-II phase matched OPAs. These authors also presented measurements of the fluorescence spectrum and the photon-counting interarrival statistics for a multi-mode type-I system. They did not, however, discuss polarization entanglement or coincidence-counting dips and revivals.

The configuration we shall consider is shown in Fig. 1(a). A type-II phase matched $\chi^{(2)}$ crystal is embedded in a single-ended, dual-cavity arrangement and subject to single-pass, continuous-wave pumping at frequency ω_P . The polarizing beam splitter in Fig. 1(a) separates the signal and idler beams so that they see identical output couplers but different free-space cavity lengths. For simplicity, we employ a collinear, plane-wave propagation model with no pump depletion, no pump fluctuations, and no excess losses. We also

assume perfect phase-matching at degeneracy—the center frequencies of the signal and idler beams are both $\omega_P/2$ —with both the signal and idler cavities resonant at this frequency.

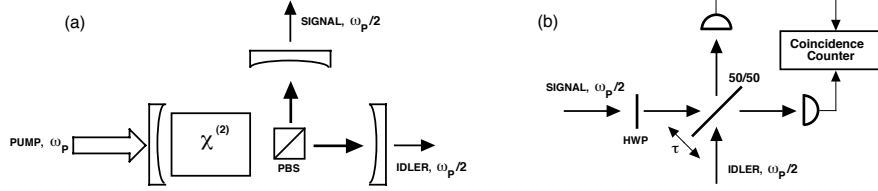


Figure 1. (a): Doubly-resonant, type-II phase matched optical parametric amplifier with continuous-wave pumping. The pump is single pass and enters through a mirror that is totally reflecting for the signal and idler. The polarizing beam splitter (PBS) separates the signal and idler so that they see identical output couplers but different optical cavities. (b): Hong-Ou-Mandel interferometer for measuring quantum interference, via coincidence counting, as the delay, τ , scanned. Because a type-II OPA is assumed, the half-wave plate (HWP) is needed to rotate the signal polarization to match that of the idler.

To analyze the Fig. 1(a) configuration, we start from the coupled-mode equations for the downconversion process without the resonators. With $\hat{E}_S(z, t)$ and $\hat{E}_I(z, t)$ denoting the positive-frequency, photon-units field operators for the relevant polarization components of the signal and idler, respectively, we have that,

$$\frac{\partial \hat{A}_S(z, \omega)}{\partial z} = i\kappa A_P \hat{A}_I^\dagger(z, \omega) e^{i\Delta k z} \quad \text{and} \quad \frac{\partial \hat{A}_I(z, \omega)}{\partial z} = i\kappa A_P \hat{A}_S^\dagger(z, \omega) e^{i\Delta k z}, \quad (1)$$

for $+z$ propagation within the nonlinear crystal, where $E_P(z, t) = A_P e^{-i(\omega_P t - k_P z)}$ is the classical pump field, and

$$\hat{E}_S(z, t) = \int \frac{d\omega}{2\pi} \hat{A}_S(z, \omega) e^{-i(\omega_P/2 + \omega)t + ik_S z}, \quad (2)$$

$$\hat{E}_I(z, t) = \int \frac{d\omega}{2\pi} \hat{A}_I(z, \omega) e^{-i(\omega_P/2 - \omega)t + ik_I z}. \quad (3)$$

In Eq. (1), κ is the nonlinear coupling coefficient, and $\Delta k \equiv k_P - k_S - k_I$ gives the phase mismatch at detuning ω in terms of the pump wave number at ω_P , the signal wave number at $\omega_P/2 + \omega$, and the idler wave number at $\omega_P/2 - \omega$. The parametric interaction entangles the signal mode at frequency $\omega_P/2 + \omega$ with the idler mode at frequency $\omega_P/2 - \omega$; our sign conventions in Eqs. (2) and (3) makes these entangled modes $\hat{A}_S(z, \omega)$ and $\hat{A}_I(z, \omega)$, respectively. Because the crystal is phase matched at degeneracy, the detuning term $e^{i\Delta k z}$ in Eq. (1) can be replaced with $e^{i\omega \Delta k' z}$, where $\Delta k' \equiv -k'_S(\omega_P/2) + k'_I(\omega_P/2)$

to lowest order in a Taylor-series expansion. For a crystal of length l , with input at $z = 0$ and output at $z = l$, we then find that,

$$\begin{aligned}\hat{A}_S(l, \omega) &= \left[\cosh(pl) - \frac{i\omega\Delta k'l \sinh(pl)}{2pl} \right] e^{i\omega\Delta k'l/2} \hat{A}_S(0, \omega) \\ &+ i\kappa A_P l \frac{\sinh(pl)}{pl} e^{i\omega\Delta k'l/2} \hat{A}_I^\dagger(0, \omega),\end{aligned}\quad (4)$$

$$\begin{aligned}\hat{A}_I(l, \omega) &= \left[\cosh(pl) - \frac{i\omega\Delta k'l \sinh(pl)}{2pl} \right] e^{i\omega\Delta k'l/2} \hat{A}_I(0, \omega) \\ &+ i\kappa A_P l \frac{\sinh(pl)}{pl} e^{i\omega\Delta k'l/2} \hat{A}_S^\dagger(0, \omega),\end{aligned}\quad (5)$$

where $p \equiv \sqrt{\kappa^2 |A_P|^2 - (\omega\Delta k'/2)^2}$. Equations (4) and (5) comprise a two-mode Bogoliubov transformation, familiar from squeezed-state theory, that is commutator preserving. In the low-gain limit, $\kappa |A_P| l \ll 1$, this transformation converts a pair of vacuum-state input fields, $\hat{E}_S(0, t)$ and $\hat{E}_I(0, t)$, into a pair of output fields, $\hat{E}_S(l, t)$ and $\hat{E}_I(l, t)$, that contains a bi-photon state, viz., the joint output state of the signal and idler is approximately,

$$|\psi\rangle_{SI} \approx |\mathbf{0}\rangle_S |\mathbf{0}\rangle_I + \int \frac{d\omega}{2\pi} i\kappa A_P l e^{-i\omega\Delta k'l/2} \frac{\sin(\omega\Delta k'l/2)}{\omega\Delta k'l/2} |\omega_P/2+\omega\rangle_S |\omega_P/2-\omega\rangle_I, \quad (6)$$

where $|\mathbf{0}\rangle$ denotes the multimode vacuum state, and $|\Omega\rangle$ denotes a single-photon state at frequency Ω . It is now easy to show that this state produces a triangular coincidence-counting dip of width $2|\Delta k'l|$, shown in Fig. 3(a), as delay is scanned in the HOM interferometer shown in Fig. 1(b).

The low-gain approximations to Eqs. (4) and (5) that lead to Eq. (6) are not commutator preserving. Thus, in our treatment of the doubly-resonant OPA, we postpone passage to the low-gain limit until after the effects of the resonant cavities have been calculated. The signal and idler cavities both resonate at $\omega_P/2$; we shall assume that their optical path lengths are the same at this frequency, i.e., $L = n_S(\omega_P/2)l + l_S = n_I(\omega_P/2)l + l_I$ in terms of the signal and idler refractive indices at degeneracy and the lengths of the free-space paths in the signal and idler cavities. Let $\hat{E}_S^{\text{in}}(t)$ and $\hat{E}_I^{\text{in}}(t)$ denote the input signal and idler field operators—assumed to be in their vacuum states—and $\hat{E}_S^{\text{out}}(t)$ and $\hat{E}_I^{\text{out}}(t)$ be the resulting output field operators for the signal and idler. Introducing the Fourier relations [cf. Eqs. (2) and (3)],

$$\hat{E}_S(t) = \int \frac{d\omega}{2\pi} \hat{A}_S(\omega) e^{-i(\omega_P/2+\omega)t} \quad \text{and} \quad \hat{E}_I(t) = \int \frac{d\omega}{2\pi} \hat{A}_I(\omega) e^{-i(\omega_P/2-\omega)t}, \quad (7)$$

for these input and output field operators, and passing to the low-gain limit, we find that joint output state of the signal and the idler is approximately,

$$|\psi\rangle_{SI} \approx |\mathbf{0}\rangle_S |\mathbf{0}\rangle_I$$

$$+ \int \frac{d\omega}{2\pi} \frac{i\kappa A_P l T e^{-i(\omega \Delta k' l/2 - \theta)}}{|1 - \sqrt{R} e^{i2\omega L/c}|^2} \frac{\sin(\omega \Delta k' l/2)}{\omega \Delta k' l/2} |\omega_P/2 + \omega\rangle_S |\omega_P/2 - \omega\rangle_I, \quad (8)$$

where θ is a physically unimportant absolute phase, and $R = 1 - T$ is the reflectivity of the output couplers. Comparing the bi-photon terms in Eqs. (6) and (8), we see that the signal and idler cavities have introduced a double-resonance denominator. Our final tasks will be to explore the implications of this denominator in narrowband pair generation, in polarization entanglement generation, and in HOM interferometry.

Our lumped-element analysis of narrowband pair generation from a doubly-resonant OPA³ predicts that the signal and idler outputs will be in a maximally-entangled state whose normally-ordered (fluorescence) spectrum versus detuning satisfies,

$$\langle \hat{A}_S^{\text{out}\dagger}(\omega) \hat{A}_S^{\text{out}}(\omega') \rangle = \langle \hat{A}_I^{\text{out}\dagger}(\omega) \hat{A}_I^{\text{out}}(\omega') \rangle = 2\pi S^{(n)}(\omega) \delta(\omega - \omega'), \quad (9)$$

with

$$S^{(n)}(\omega) = [2G\Gamma^2/(\omega^2 + \Gamma^2)]^2, \quad (10)$$

where the last equality assumes operation in the low-gain regime, Γ is the common linewidth of the signal and idler cavities, and G^2 is the OPA pump power divided by the threshold power for oscillation. The corresponding fluorescence spectrum obtained from Eq. (8) of our traveling-wave theory is,

$$S^{(n)}(\omega) = \frac{|\kappa A_P l T|^2}{|1 - \sqrt{R} e^{i2\omega L/c}|^4} \left(\frac{\sin(\omega \Delta k' l/2)}{\omega \Delta k' l/2} \right)^2 \quad (11)$$

$$\approx \frac{|\kappa A_P l T|^2}{[(2\omega L/c)^2 + (1 - \sqrt{R})^2]^2}, \quad (12)$$

where the approximation assumes high- Q cavities and $|\omega| \ll \pi c/L \ll 2\pi/|\Delta k' l|$. With the identifications $\Gamma = c(1 - \sqrt{R})/2L$ and $G = \kappa |A_P| l T / 2(1 - \sqrt{R})^2$, we see that the traveling-wave and lumped-element OPA analyses coincide.

To obtain the high-brightness narrowband source of polarization-entangled photon pairs needed for our long-distance teleportation architecture,¹ we combine the signal beams and the idler beams from from a pair of Fig. 1(a) configuration doubly-resonant OPAs on a polarizing beam splitter, as shown in Fig. 2. We have previously used lumped-element analysis³ to demonstrate that the Fig. 2 arrangement produces the desired singlet-state polarization entanglement when the OPAs are pumped π -rad out of phase. The traveling-wave treatment we have developed in the present paper affords a more complete understanding of the entangled state that is produced by the Fig. 2 setup. In particular, from Eq. (8) we find that the joint output state of the signal and idler in the low-gain regime is,

$$|\psi\rangle_{SI} \approx |\mathbf{0}\rangle_{S_x} |\mathbf{0}\rangle_{I_y} |\mathbf{0}\rangle_{S_y} |\mathbf{0}\rangle_{I_x}$$

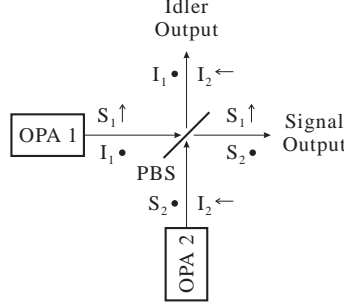


Figure 2. Type-II OPA configuration for generating polarization-entangled photon pairs. Each OPA is a doubly-resonant configuration, as shown in Fig. 1(a). The two OPAs are coherently pumped π -rad out of phase, to produce the singlet state needed for qubit teleportation. For each optical beam, the propagation direction is \hat{z} , and \hat{x} and \hat{y} polarizations are denoted by arrows and bullets, respectively. PBS, polarizing beam splitter.

$$+ \int \frac{d\omega}{2\pi} S^{(p)}(\omega) (|\omega_P/2 + \omega\rangle_{S_x} |\omega_P/2 - \omega\rangle_{I_y} - |\omega_P/2 + \omega\rangle_{S_y} |\omega_P/2 - \omega\rangle_{I_x}), \quad (13)$$

where

$$S^{(p)}(\omega) \equiv \frac{i\kappa A_P l T e^{-i(\omega\Delta k' l/2 - \theta)} \sin(\omega\Delta k' l/2)}{|1 - \sqrt{R} e^{i2\omega L/c}|^2 \omega\Delta k' l/2}, \quad (14)$$

is the phase-sensitive spectrum. Equation (13) shows the singlet-state behavior that enables qubit teleportation. Moreover, because the Lloyd et al. quantum memory² will only respond to the narrowband portion of the biphoton field in the vicinity of the ^{87}Rb line, we can reproduce the teleportation performance analysis of Ref. 1—which employed lumped-element OPA theory—by matching the double resonance at $\omega_P/2$ to the ^{87}Rb line center.

Finally, let us revisit HOM interferometry when the signal and idler inputs come from a doubly-resonant OPA. When the state Eq. (8) is supplied to the interferometer in Fig. 1(b), a series of triangular coincidence-counting dips and revivals occur. The width of each dip is set by the phase-matching bandwidth, i.e., each dip is $2|\Delta k' l|$ wide, just as found for the non-resonated downconverter. The spacing between each coincidence dip is $2L/c$, i.e., a cavity roundtrip. The central (deepest) coincidence dip is as shown in Fig. 3(a) for the non-resonated case. The remaining coincidence dips become progressively shallower as the delay is scanned further from the location of the central dip. The span of the dips-and-revivals region is many cavity lifetimes—for our high- Q , no-excess-loss cavities—as shown by the envelope of their maxima and minima which is plotted in Fig. 3(b). This new quantum interference phenomenon has a simple physical explanation. Signal and idler photon pairs are

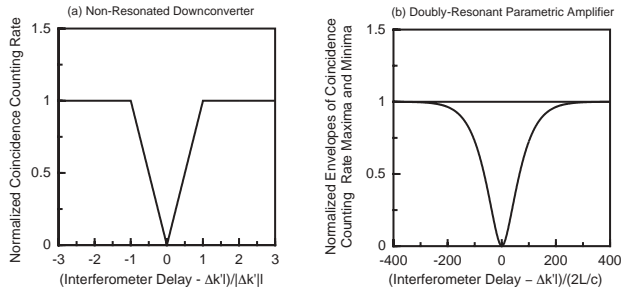


Figure 3. (a): Normalized coincidence-counting rate versus delay for a Hong-Ou-Mandel interferometer whose input is the output state from a (non-resonated) type-II parametric downconverter. The coincidence dip occurs at $\Delta k'l$ and is of width $2|\Delta k'l|$ (b): Envelopes of the coincidence counting rate maxima and minima for a Hong-Ou-Mandel interferometer whose input is the output state from a type-II doubly-resonant optical parametric amplifier with a 5% output coupler ($R = 0.95$). Within these envelopes, triangular coincidence dips occur every $2L/c$ from the central dip at $\Delta k'l$.

created, via parametric downconversion in the $\chi^{(2)}$ crystal, in near simultaneity. Because the crystal is embedded in high- Q cavities that resonate both the signal and idler, each photon in a particular pair will take many cavity lifetimes to leak out through its respective output coupler. A pair from a downconverter (without a resonator) gives rise to a coincidence-counting dip in a HOM interferometer when the delay is adjusted so that indistinguishable photon wave packets present themselves at the two input ports of the interferometer's beam splitter. Because of the optical cavities in the Fig. 1(a) configuration, such interference occurs at a multiplicity of delay settings—separated by multiples of the roundtrip cavity delay—as the component photons of each generated pair leak out of the OPA. In more mathematical terms, the optical cavities have imposed a comb-like structure on the common fluorescence spectrum of the signal and idler beams, and this combs lead to a similar comb-like behavior in the coincidences-versus-delay pattern seen in the HOM interferometer because the latter is in essence a Fourier transform of the former.

References

1. J. H. Shapiro, *New J. Phys.* 4:47 (2002).
2. S. Lloyd, M. S. Shahriar, J. H. Shapiro, and P. R. Hemmer, *Phys. Rev. Lett.* 87:167903 (2001).
3. J. H. Shapiro and N. C. Wong, *J. Opt. B: Quantum and Semiclass. Opt.* 2:L1 (2000).
4. C. K. Hong, Z. Y. Ou, and L. Mandel, *Phys. Rev. Lett.* 59:2044 (1987).
5. Y. J. Lu and Z. Y. Ou, *Phys. Rev. A* 62:033804 (2000).